# Accurate Analytical Modeling for Switching Energy of PiN Diodes Reverse Recovery

Saeed Jahdi, *Student Member, IEEE,* Olayiwola Alatise, Li Ran, *Senior Member, IEEE* and Philip Mawby, *Senior Member, IEEE*

***Abstract*—PiN diodes are known to contribute significantly to switching energy as a result of reverse recovery charge during turn-OFF. At high switching rates, the overlap between the high peak reserve recovery current and the high peak voltage overshoot contributes to significant switching energy. The peak reverse recovery current depends on the temperature and switching rate whereas the peak diode voltage overshoot depends additionally on the stray inductance. Furthermore, the slope of the diode turn-OFF current is constant at high IGBT switching rates and varies for low IGBT switching rates. In this paper, an analytical model for calculating PiN diode switching energy at different switching rates and temperatures is presented and validated by ultra-fast and standard recovery diodes with different current ratings. Measurements of current commutation in IGBT/PiN diode pairs have been made at different switching rates and temperatures and used to validate the model. It is shown here that there is an optimal switching rate to minimize switching energy. The model is able to correctly predict the switching rate and temperature dependence of the PiN diode switching energies for different devices.**

***Index Terms*—PiN Diodes, Reverse Recovery, Switching Transient, Switching Energy, Analytical Modeling**

## NOMENCLATURE

| | |
|---|---|
| $I_F$ | Forward Current (A) |
| $I_{RR}$ | Peak Reverse Recovery Current (A) |
| $dI_{TF}/dt$ | Overall *dI/dt* of turn-OFF current at high *dI/dt* (A/s) |
| $dI_{TF+}/dt$ | *dI/dt* of turn-OFF current before zero-crossing (A/s) |
| $dI_{TF-}/dt$ | *dI/dt* of turn-OFF current after zero-crossing (A/s) |
| $dI_{RR}/dt$ | Primary *dI/dt* of recovery current (A/s) |
| $dI_{Tail}/dt$ | Secondary *dI/dt* of recovery tail current (A/s) |
| $d^2I_{TF}/dtdT$ | Primary *dI/dt* of recovery current (A/s°C) |
| $E_{SW}$ | Switching Energy (J) |
| $V$ | Absolute value of the switching voltage (V) |
| $V_{AK}$ | Diode peak overshoot (V) |
| $V_D$ | Absolute value of the Diode on-state voltage drop (V) |
| $L$ | Stray parasitic inductance (H) |
| $K_Q$ | Function of junction temperature ($C/A^{0.5}$) |
| $K$ | Ratio of *dI/dt* of recovery current to turn-OFF |
| $S$ | Ratio of the Recovery time to the turn-OFF time as a measure of the diode snappiness [1] |
| $t$ | Time (s) |
| $T$ | Temperature (°C) |

Manuscript received January 3, 2014; revised April 28, 2014 and May 19, 2014; accepted May 22, 2014.



This research has been funded by the Engineering and Physical Science Research Council (EPSRC) through the Underpinning Power Electronics Devices Theme (EP/L007010/1) and the Components Theme (EP/K034804/1).

The authors are with the Department of Electrical and Electronics Engineering, School of Engineering, University of Warwick, Coventry, West Midlands, CV4 7AL, United Kingdom (e-mail: s.jahdi@warwick.ac.uk, o.alatise@warwick.ac.uk, l.ran@warwick.ac.uk, p.a.mawby@warwick.ac.uk)

## I. INTRODUCTION

POWER PiN diodes are a critical device technology for power conversion both for automotive and grid connected applications. Although SiC Schottky diodes have increasingly become popular as a replacement for silicon PiN diodes, as far as power conversion at very high levels and medium frequencies are concerned, silicon PiN diodes remain unrivalled in delivering low conduction on-state energy dissipation. These diodes are commonly used as anti-parallel diodes with IGBTs or MOSFETs in self-commutated voltage-source converters. In power conversion applications where low switching frequencies are to be used, e.g. MMC-VSC for off-shore wind power transmission, PiN diodes remain the technology of choice for low conduction on-state energy dissipation. Also, SiC PiN diodes have been demonstrated with very high voltage blocking capability [2]. PiN diodes are bipolar devices that rely on conductivity modulation from minority carrier injection to deliver low conduction on-state energy dissipation. As a result, minority carrier recombination and recovery during switching periods limits the maximum switching frequency that can be used in power conversion. The reverse recovery charge during the turn-OFF of the PiN diode is known to be the highest contributing factor to switching energy in PiN diodes. Furthermore, the diode voltage overshoot arising from stray inductances also contributes to the switching energy. Both the peak reverse recovery current and voltage overshoot increase with the *dI/dt* which is controlled by the RC time constant of the IGBT. The diode parasitic capacitance and circuit stray inductance will also determine the rate that the diode ramps down the current.

Models developed for the PiN diode's reverse recovery transients fall mainly into two categories; physics-based SPICE models (which require device physics parameters) and analytical models that are based on waveform characterizations. The SPICE sub-circuit models for reverse recovery behavior of PiN diodes are mainly physics-based and hence, depend on device parameters. The physics of

PiN diodes are described in [3]–[9] whereas some of the SPICE models are provided in [10]–[16]. SPICE models are accurate in modelling PiN diodes, although prior knowledge of all device parameters is required which may be hindered by the fact that some of them are not on the manufacturers' datasheet. Hence, although SPICE models are useful in understanding the PiN diodes' transient performance [17] and reliability [18], waveform based approaches can be a fast and reliable method of predicting the switching performance of PiN diodes under different conditions given a few initial measurements [19]–[22].

In this paper, an analytical model is developed to calculate the switching energy of the PiN diode as a function of the circuit *dI/dt* and temperature. This model has been validated experimentally and has been shown to be accurate over a wide range of *dI/dt* and temperatures. It accounts for the dependence of the peak reverse recovery current and the peak diode voltage overshoot on *dI/dt* and is able to predict the switching energy of the diode accurately. The model also correctly predicts the dependency of the switching energy on temperature. Implementing the model will require *dI/dt*, *dV/dt* and their temperature dependencies as input parameters which may mean that some experimental characterization is required at the outset if not known. However, once known, the model is capable of predicting the switching energy accurately for different switching conditions without using detailed device parameters that are not given. Section II details the development of this switching energy model, Section III explains the experimental measurements that are used to validate the model, Section IV discusses the comparison between the measured and modeled switching energies while Section V concludes the paper.

## II. Model Development

To develop a comprehensive model consistent with the results of experimental measurements performed in next section, the behavior of the PiN diode at turn off should be first analyzed. Figure 1 shows a typical turn-OFF switching transient of a 1.2 kV/40 A silicon PiN diode switched at 2 different rates. It can be seen that the reverse recovery current and the diode voltage overshoot will contribute significantly to the switching energy. In the on-state, the voltage across the diode is determined by the carrier distribution profile within the drift region and the voltage drop across the P-N and N-N junctions. As the diode is turned-off, the excess charge in the drift region is reduced by recombination and diffusion. The current through the diode ramps down at a rate of *dI/dt* and crosses the zero mark before reaching the peak reverse current. As the voltage across the diode crosses zero and the diode becomes reverse biased, depletion regions form across the junctions of the diode thereby cutting off the supply of minority carriers from the highly doped regions into the drift region. The charge profile within the diode becomes unable to support the current through the diode as a result of the extending depletion widths formed by the reverse bias voltage, hence, the current starts returning to zero. As a result, the slope of the current changes polarity and the diode goes into reverse recovery. At this point, the lifetime of the minority carriers in the drift region of the diode determines the duration of the switching transient.

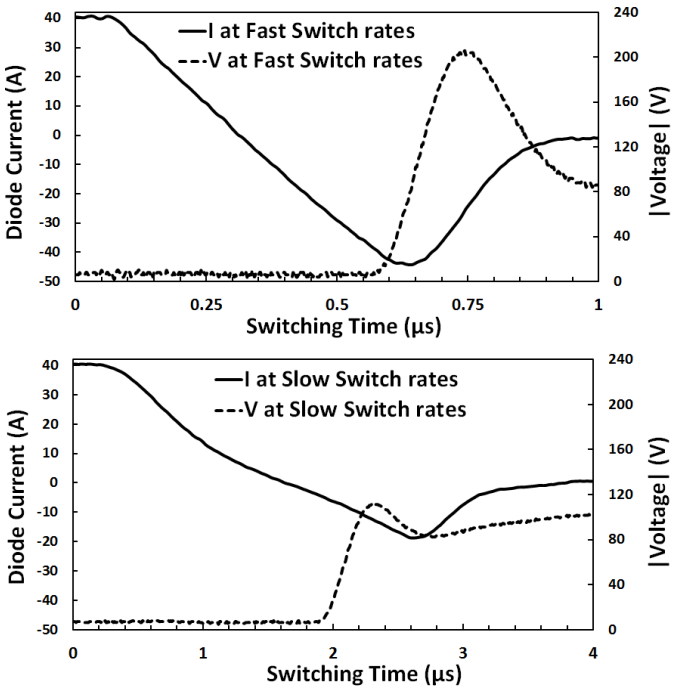


Fig. 1. Typical turn-OFF transients of PiN Diode in different switching rates.

For the purpose of this paper, the switching energy ($E_{SW}$) is defined by:

$$E_{SW} = \int_0^t V_{AK}(t) i_D(t) dt \tag{1}$$

where t is the total duration of the switching transient. Here, 0 is when the current starts ramping down whereas *t* is defined as the time instant when the reverse recovery current returns to zero (this is shown clearer in the model development section). It should be noted that this model only studies the turn-OFF transient, therefore, due to the possible stored energy in the PiN diode, the supplied power cannot be considered to be exact equal of the power losses (dissipated heat). When modelling the switching energy of a PiN diode, it has previously been assumed that *dI/dt* is constant before and after the zero-crossing of the reverse current and the *dI/dt* is constant throughout the recombination phase. However, the experimental measurements in section III will show that when the IGBT is switched at lower rates (using higher gate resistances), the slope of the current is not constant. Figure 1 shows the measured diode current for the same PiN diode with two different switching rates. It can be seen from Figure 1 that the turn-OFF current at a slow switching rate has 2 distinctive slopes whereas that at a high switching rate has a single slope. The switching voltage has been accounted for as the absolute value of the voltage. This assumption results in considerable simplification of the model, although it has a slight adverse effect on the model's output accuracy. It has also previously been assumed that the voltage and current waveforms can be considered linear and the energy can be calculated from the

area of the overlap of current/voltage [23]–[26] and hence, the switching energy ($E_{SW}$) is simply the area of the triangle formed by the linear over-lapping transients. This switching energy has sometimes been expressed in the capacitance charge ($0.5Q_cV$) or IV ($0.5IVt$). Applying this method to the calculation of the turn-OFF switching energy of PiN diode normally results in a considerable margin of error. This is shown in Figure 2. This method yields:

$$I_{RR} = \sqrt{\frac{\mathrm{d}I_{TF}}{\mathrm{d}t}\frac{2k_Q\sqrt{I_F}}{1+S}} \quad \text{and} \quad V_{AK} = V + L\frac{\mathrm{d}I_{RR}}{\mathrm{d}t} \tag{2}$$

$$E_{SW} = \frac{1}{2}\sqrt{\frac{2k_Q\sqrt{I_F}}{1+S}}\sqrt{\frac{\mathrm{d}I_{TF}}{\mathrm{d}t}}\left(V + L\frac{\mathrm{d}I_{RR}}{\mathrm{d}t}\right)\left(\frac{I_F + I_{RR}}{\frac{\mathrm{d}I_{TF}}{\mathrm{d}t}} + \frac{I_{RR}}{\frac{\mathrm{d}I_{RR}}{\mathrm{d}t}}\right) \tag{3}$$

Equation (2) expresses the peak reverse recovery current ($I_{RR}$) as a function of the turn-OFF switching rate ($dI_{TF}$/dt), the derivation of which is in [27]. In (2), S is a measure of the softness of the diode's recovery (ratio of the time between the zero crossing of the current and the peak reverse current to the time between the peak of the current and the zero) and $k_Q$ is a function that defines the relationship between the stored charge in the diode and the forward current ($I_F$) [1], [27]. It also accounts for the diode voltage ($V_{AK}$) plus the peak inductive voltage overshoot ($LdI_{RR}$/dt) resulting from the product of the switching rate and the parasitic inductance of the diode ($L$). Equation (3) is the switching energy of the diode ($E_{SW}$) expressed as a product of the peak reverse current, the peak diode voltage and the switching time. The total switching time is expressed as the sum of the time required for the current to fall from the $I_F$ to the peak reverse current ($I_F$+$I_{RR}$)/($dI_{TFF}$/dt) and the time taken for the current to go from the peak reverse current back to zero ($I_{RR}$)/($dI_{RR}$/dt). Figure 2 shows the result of this method in comparison with a measurement taken from the 1.2 kV/40 A diode switched with $R_G$ = 22 Ω.

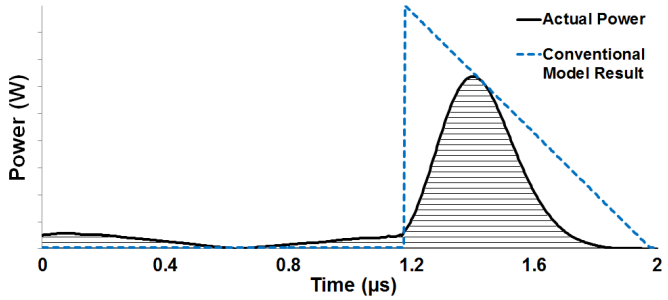


Fig. 2. Conventional methods of transient energy calculations showing inconsistency with Actual Power output of P-i-N diode

As seen in Figure 2, there is some error as a result of the simplistic triangular approximation of the switching power. This results in an over-estimation of the switching energy. Therefore to have a more accurate analytical calculation of PiN diodes switching energy during reverse recovery, a less simplistic linearized waveform model is used. Figure 3 shows a linear approximation of the voltage and current waveforms of Figure 1 and the resultant approximation of the instantaneous power. In Figure 3, the negative *dV'/dt* is half of the positive *dV/dt* and $\Delta t$ accounts for the time difference between the peak reverse current and the rise of the diode voltage. Figure 1 shows that the slope of the PiN diode's turn-OFF current is constant at high switching rates meaning:

$$\frac{\mathrm{d}I_{TF+}}{\mathrm{d}t} = \frac{\mathrm{d}I_{TF-}}{\mathrm{d}t} \quad \text{and} \quad \frac{\mathrm{d}I_{RR}}{\mathrm{d}t} = \frac{\mathrm{d}I_{Tail}}{\mathrm{d}t}$$

This should be applied after removing $E_{SW5}$ from Figure 3.

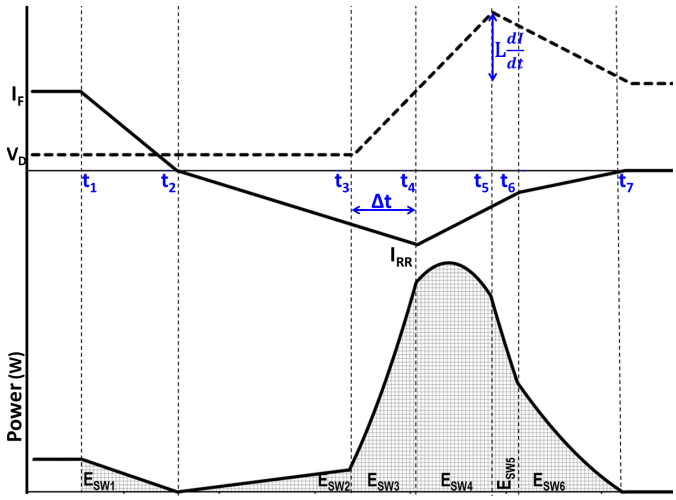


Fig. 3. Linearized current and voltage waveforms showing reverse recovery, inductive voltage overshoot and the profile of the dissipated power. Here, 2 slopes are used in the diode current both during recovery and recombination. This can be simplified for lower gate resistances.

As can be seen from Figure 3, the switching power is comprised of 6 areas, the sum of which will yield the total switching energy of the PiN diode. It is clear that the profile of the switching power in Figure 3 is a closer approximation of the actual measurement in Figure 2. The total switching energy can be calculated using equations below:

$$E_{SW} = |E_{SW_1}| + |E_{SW_2}| + \sum_{n=3}^{6}|E_{SW_n}| \tag{4}$$

$$E_{SW_1} = \frac{I_F^2 V_D}{2\left(\frac{\mathrm{d}I_{TF+}}{\mathrm{d}t}\right)} \tag{5}$$

$$E_{SW_2} = \frac{V_D}{2}\left(I_{RR} - \Delta t\frac{\mathrm{d}I_{TF-}}{\mathrm{d}t}\right)\left(\frac{I_{RR}}{\frac{\mathrm{d}I_{TF-}}{\mathrm{d}t}} - \Delta t\right) \tag{6}$$

$$E_{SW_n} = \frac{a_n b_n}{3}\left(t_{n+1}^3 - t_n^3\right) + \frac{a_n d_n + b_n c_n}{2}\left(t_{n+1}^2 - t_n^2\right) + b_n d_n\left(t_{n+1} - t_n\right) \tag{7}$$

The switching time intervals defined in Figure 3 can be calculated as:

$$t_1 = 0 \quad \text{and} \quad t_2 = \frac{I_F}{\frac{\mathrm{d}I_{TF+}}{\mathrm{d}t}}$$

$$t_3 = \frac{I_F}{\frac{\mathrm{d}I_{TF+}}{\mathrm{d}t}} + \frac{I_{RR}}{\frac{dI_{TF-}}{dt}} - \Delta t \quad \text{and} \quad t_4 = \frac{I_F}{\frac{\mathrm{d}I_{TF+}}{\mathrm{d}t}} + \frac{I_{RR}}{\frac{dI_{TF-}}{dt}}$$

$$t_5 = \frac{I_F}{\frac{\mathrm{d}I_{TF+}}{\mathrm{d}t}} + \frac{I_{RR}}{\frac{dI_{TF-}}{dt}} - \Delta t + \frac{V + L\frac{\mathrm{d}I_{RR}}{\mathrm{d}t} - V_D}{\frac{\mathrm{d}V}{\mathrm{d}t}}$$

$$t_6 = \frac{I_F}{\frac{\mathrm{d}I_{TF+}}{\mathrm{d}t}} + \frac{I_{RR}}{\frac{dI_{TF-}}{dt}} + \frac{\frac{\mathrm{d}I_{Tail}}{\mathrm{d}t}\left(\frac{V + \frac{3}{2}\left(L\frac{\mathrm{d}I_{RR}}{\mathrm{d}t}\right) - V_D}{\frac{\mathrm{d}V}{\mathrm{d}t}} - \Delta t\right) - I_{RR}}{\frac{\mathrm{d}I_{Tail}}{\mathrm{d}t} - \frac{\mathrm{d}I_{RR}}{\mathrm{d}t}}$$

$$t_7 = \frac{I_F}{\frac{\mathrm{d}I_{TF+}}{\mathrm{d}t}} + \frac{I_{RR}}{\frac{dI_{TF-}}{dt}} - \Delta t + \frac{V + \frac{3}{2}L\frac{\mathrm{d}I_{RR}}{\mathrm{d}t} - V_D}{\frac{\mathrm{d}V}{\mathrm{d}t}}$$

and the coefficients of equation(7) can be calculated as:

$$a_3 = -\frac{\mathrm{d}I_{TF-}}{\mathrm{d}t} \quad , \quad a_4 = \frac{\mathrm{d}V}{\mathrm{d}t} \quad , \quad a_5 = \frac{\mathrm{d}I_{RR}}{\mathrm{d}t} \quad , \quad a_6 = -\frac{\mathrm{d}V}{2dt}$$

$$c_3 = \frac{\mathrm{d}V}{\mathrm{d}t} \quad , \quad c_4 = \frac{\mathrm{d}I_{RR}}{\mathrm{d}t} \quad , \quad c_5 = -\frac{\mathrm{d}V}{2dt} \quad , \quad c_6 = \frac{\mathrm{d}I_{Tail}}{\mathrm{d}t}$$

$$b_3 = \frac{\mathrm{d}I_{TF-}}{\mathrm{d}t}\left(\frac{I_F}{\frac{\mathrm{d}I_{TF+}}{\mathrm{d}t}} + \frac{I_{RR}}{\frac{\mathrm{d}I_{TF-}}{\mathrm{d}t}}\right) - I_{RR}$$

$$b_4 = d_3 = V_D - \frac{\mathrm{d}V}{\mathrm{d}t}\left(\frac{I_F}{\frac{\mathrm{d}I_{TF+}}{\mathrm{d}t}} + \frac{I_{RR}}{\frac{\mathrm{d}I_{TF-}}{\mathrm{d}t}} - \Delta t\right)$$

$$b_5 = d_4 = -\frac{\mathrm{d}I_{RR}}{\mathrm{d}t}\left(\frac{I_F}{\frac{\mathrm{d}I_{TF+}}{\mathrm{d}t}} + \frac{I_{RR}}{\frac{\mathrm{d}I_{TF-}}{\mathrm{d}t}}\right) - I_{RR}$$

$$b_6 = d_5 = \frac{3}{2}\left(V + L\frac{\mathrm{d}I_{TF-}}{\mathrm{d}t}\right) + \frac{\mathrm{d}V}{2dt}\left(\frac{I_F}{\frac{\mathrm{d}I_{TF+}}{\mathrm{d}t}} + \frac{I_{RR}}{\frac{\mathrm{d}I_{TF-}}{\mathrm{d}t}} - \frac{V_D}{\frac{\mathrm{d}V}{\mathrm{d}t}} - \Delta t\right)$$

$$d_6 = -\frac{\mathrm{d}I_{Tail}}{\mathrm{d}t}\left(\frac{V + \frac{3}{2}L\frac{\mathrm{d}I_{TF-}}{\mathrm{d}t} - V_D}{\frac{\mathrm{d}V}{\mathrm{d}t}}\right) - \frac{\mathrm{d}I_{Tail}}{\mathrm{d}t}\left(\frac{I_F}{\frac{\mathrm{d}I_{TF+}}{\mathrm{d}t}} + \frac{I_{RR}}{\frac{\mathrm{d}I_{TF-}}{\mathrm{d}t}} - \Delta t\right)$$

To make the model temperature compliant, the temperature dependence of the PiN diodes has to be incorporated into the model. The slope of the diode turn-OFF current ($dI_{TF}/dt$) reduces with increasing temperature and the peak reverse current increases with temperature due to the higher carrier lifetime. These dependencies can modelled from experimental measurements of diode reverse current waveforms at different temperatures. The diode peak voltage overshoot due to parasitic inductance reduces as the temperature is increased. This is due to the negative temperature coefficient of the switching rate since the product of the switching rate and the parasitic inductance will yield the voltage overshoot. The equations that will account for these temperature dependencies of the switching rate, the peak diode voltage overshoot and the peak reverse recovery current as shown below in equations (8), (9) and (10):

$$\frac{\mathrm{d}I_{TF}}{\mathrm{d}t} = \frac{\mathrm{d}I_{TF}}{\mathrm{d}t}^{(25^\circ\mathrm{C})} - \frac{\mathrm{d}^2 I_{TF}}{\mathrm{d}t\,\mathrm{d}T}(T - 25) \tag{8}$$

$$V_{AK} = V^{(25^\circ\mathrm{C})} - \frac{\mathrm{d}V}{\mathrm{d}T}(T - 25) \tag{9}$$

$$I_{RR} = I_{RR}{}^{(25^\circ\mathrm{C})} + \frac{\mathrm{d}I_{TF}}{\mathrm{d}T}(T - 25) \tag{10}$$

The next section, details the experimental measurements that will be used to validate the model.

## III. Clamped Inductive Switching Measurements

The classical clamped inductive switching circuit has been used to determine the switching energy and reverse recovery characteristics of the PiN diodes. Figure 4 shows the circuit schematic while the actual test rig is shown in [28]–[30]. This arrangement comprises of a low side switching IGBT and a high side PiN diode. The IGBT is switched on initially to charge the inductor after which it is switched off so the current can free-wheel through the PiN diode. The IGBT is then switched on so that the current can commutate from the diode to the IGBT and turn-OFF characteristics of the diode can be observed. The procedure is performed for different switching rates (by using different gate resistances) and with different ambient temperatures. Switching waveforms are captured on a Tektronix TDS5054B digital phosphor oscilloscope which has a bandwidth of 500 MHz. The current is measured using a Tektronix TCP303 current probe which is connected to the oscilloscope through a TCPA300 amplifier. It is calibrated on a scale 20 mV/A. The voltage probes are also from Tektronix (P5210) and were scaled on a basis of 1/100.

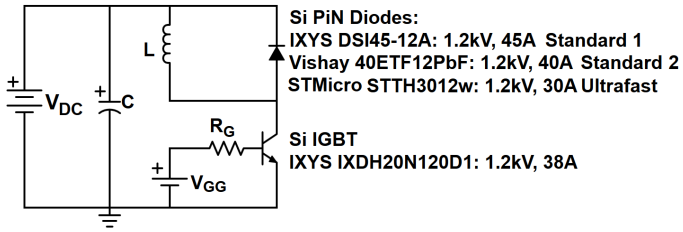


Fig. 4. Schematic of the 2-Pulse Clamped Inductive Switching Rig, DUTs are 3 different PiN Diodes with part numbers as shown.

### A. Diode Temperature Dependencies

Figure 5 shows the measured switching rate (rate of change of current with time) as a function of the gate resistance for different temperatures during the turn-ON of the IGBT and the turn-OFF of the diode. As can be seen, increasing the gate resistance has the effect of reducing *dI/dt* which is expected since the electrical time constant (product of $R_G$ and the miller capacitance of the device) increases with the gate resistance. It is also seen that the *dI/dt* decreases with increasing temperature which is in contrast to MOSFETs where *dI/dt* increases with temperature. For the IGBT to turn-ON, the charge storage region must first be populated by stored charge and since carrier lifetime increases with temperature and mobility decreases, the rate at which the IGBT will turn on will decrease with temperature. In other words, the rate of charge storage formation in the drift region decreases as the temperatures increases. This temperature-dependency is the dominant factor at high *dI/dt* (where a low $R_G$ is placed on the low-side IGBT); however with an increase in gate resistance, $R_G$ becomes the dominant factor in determining the *dI/dt* thereby suppressing the temperature effect.

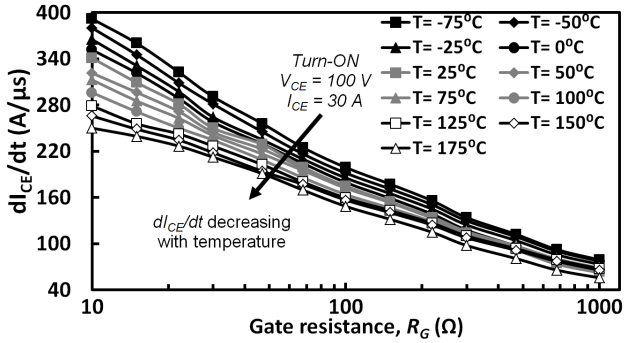


Fig. 5. The turn-ON *dI/dt* of the IGBT as a function of gate resistance.

Figure 6 shows the turn-OFF *dI/dt* of the IGBT (turn-ON of the diode) as a function of the gate resistance for different temperatures. As can be seen from Figure 6, the switching rate reduces with increasing temperature as was the case with the turn-ON characteristics.

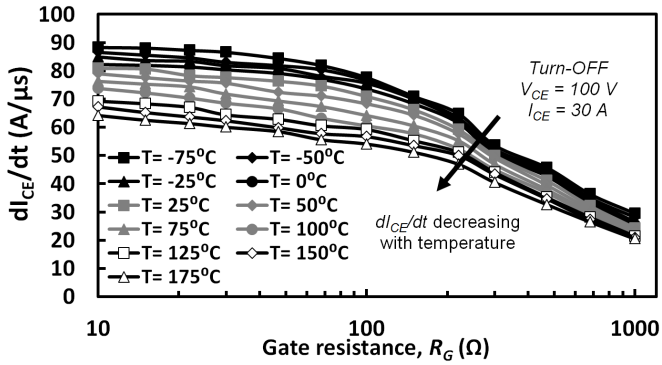


Fig. 6. The turn-OFF *dI/dt* of the IGBT as a function of the gate resistances.

The temperature dependence of the peak reverse current, the switching rate and peak diode voltage overshoot have been used to parameterize equations (8), (9), (10). The rate of change of the switching rate with temperature is extracted from the experimental measurements simply by taking the derivative of *dI/dt* with respect to temperature, thereby yielding the 2nd order derivative of the current with respect to time and temperature ($d^2I/dtdT$). This parameter has been plotted as a function of the gate resistance in Figure 7 for the 3 discrete PiN diodes shown in Figure 4. Because *dI/dt* decreases as temperature increases as a result of increased carrier lifetime with temperature, $d^2I/dtdT$ is negative as can be seen in Figure 7. It can also be seen from Figure 7 that the magnitude of $d^2I/dtdT$ slightly decreases with the gate resistance. The reduction in the absolute value of the 2nd derivative is due to the effect of large $R_G$ (slower current commutation) dominating over the impact of temperature on *dI/dt*. The rate of change of $d^2I/dtdT$ with $R_G$ is low enough for it to be considered constant without reducing the accuracy of the model. In section IV of the paper, subsequent comparisons of the model's results with experimental measurements will show this to be the case. The implication is as follows; if the rate of change of the switching rate (*dI/dt*) with temperature is known, this can be used to accurately predict the switching energy of the diode when it is switched at different rates and temperatures. Hence, Figure 7 is used to parameterize equation (8). Figure 8 shows the temperature dependence of the peak reverse recovery current and the peak diode voltage overshoot of the PiN diode when the low side IGBT is switched with a gate resistance of 22 Ω. As can be seen in Figure 8, the peak reverse recovery current has a positive temperature coefficient whereas the peak diode voltage overshoot has a negative temperature coefficient. The peak diode voltage overshoot dependence on temperature is used to parameterize equation (9) whereas the temperature dependence of the peak reverse current is used to parameterize equation (10).

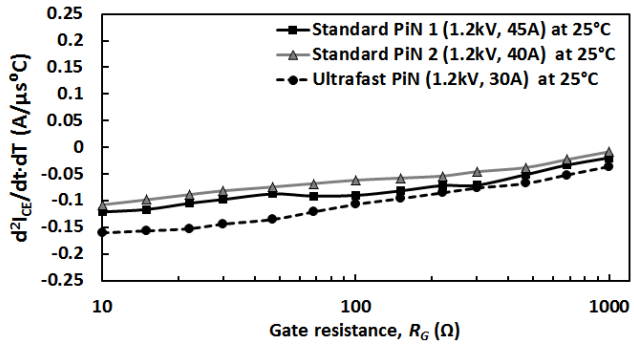


Fig. 7. $d^2I/dtdT$ as a function of gate resistance for IGBT turn-on.

### B. Diode Switching Rate Dependencies

Next, the dependence of the peak currents/voltages and switching energy on the switching rates is investigated. A wide range of gate resistances have been used to switch the low side IGBT so that a wide range of $dI_{TF}/dt$ can be used for the purpose of validating the model. Figure 9 (a) shows the impact of increasing the switching rate on the reverse recovery characteristics of the PiN diode. It is seen that the peak reverse recovery current ($I_{RR}$) increases with the $dI_{TF}/dt$ and the recovery time reduces with increasing $dI_{TF}/dt$ i.e. the diode snappiness increases with $dI_{TF}/dt$. Figure 9 (b)

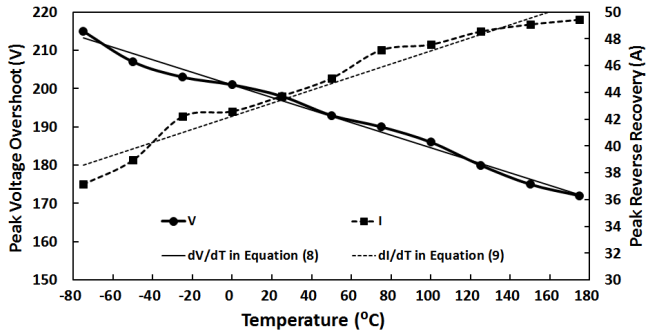


Fig. 8. Peak reverse recovery current and the peak diode voltage overshoot as functions of temperature for $R_G$ = 22 Ω

shows the diode switching voltage transients as a function of the $dI_{TF}/dt$. It is seen that the peak diode voltage overshoot also increases with $dI_{TF}/dt$. Figure 9 (c) shows a plot of the switching power for different switching rates. It is seen that the peak power increases with $dI_{TF}/dt$, although the width of the power pulse increases as $dI_{TF}/dt$ is reducing. Hence, there is opposition between the peak of the power pulse and its width as the former increases with the switching rate while the latter reduces if the switching rate is reduced. Furthermore, at some point the increase in the width of the power pulse causes the switching energy to start increasing, hence, there is an optimum switching rate for the minimization of switching energy. Figure 9 (d) shows the switching power pulse as a function of time for different temperatures at a fixed switching rate. It is seen that the peak of the pulse increases with temperature, which is due to the high peak reverse recovery current as a function of increased lifetime with temperature.

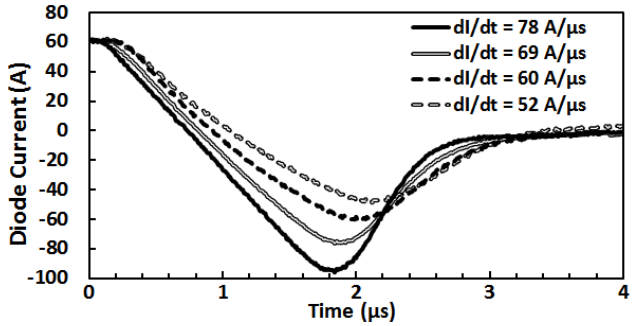


Fig. 9 (a). PiN Diode Reverse recovery Current as a function of the switching rate 25 °C with $I_F$ = 60 A for standard diode 1 (IXYS DSI45-12A).

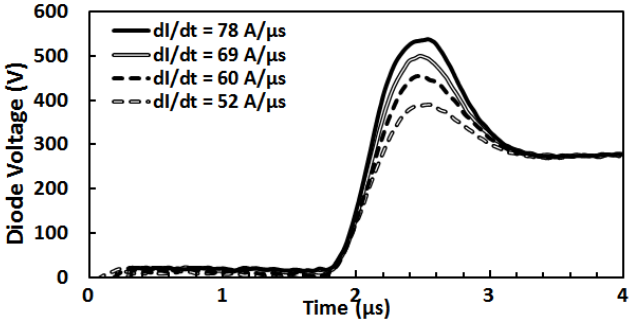


Fig. 9 (b). PiN Diode switching voltage as a function of the switching rate at 25 °C at 300 V for standard diode 1 (IXYS DSI45-12A).

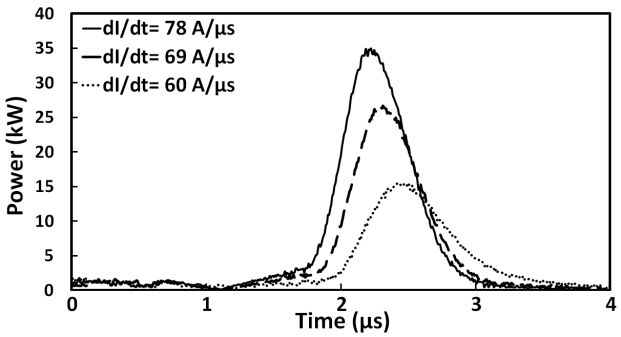


Fig. 9 (c). PiN Diode turn-OFF switching power at different switching rates at 25 °C with 300 V and 60 A for standard diode 1 (IXYS DSI45-12A).

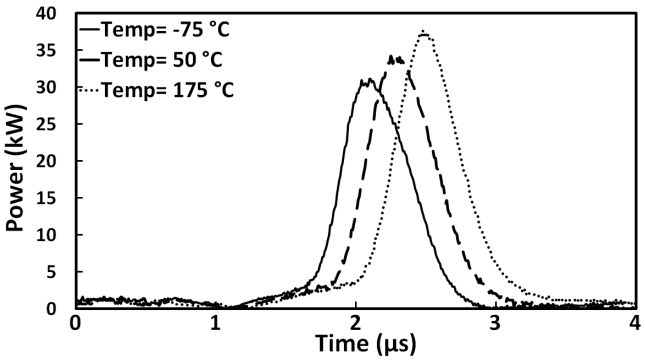


Fig. 9 (d). PiN Diode turn-OFF switching power at different temperatures with $R_G$ = 10 Ω at 300 V and $I_F$ = 60 A for standard diode 1 (IXYS DSI45-12A).

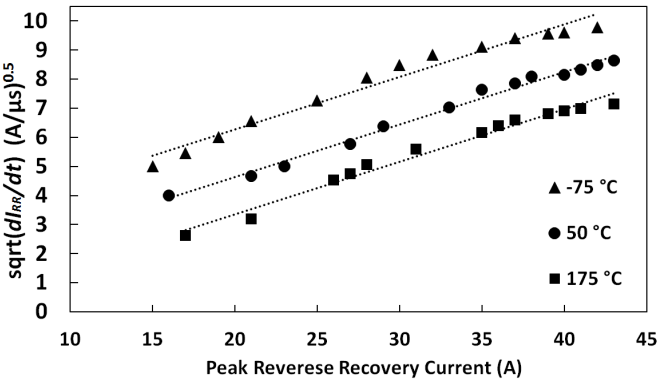


Fig. 10. Square root of $dI_{TF}/dt$ as a function of the peak reverse current showing straight lines at different temperatures.

Equation (2), which expresses the peak reverse recovery current as a function of the square root of $dI_{TF}/dt$, was developed as a model that could predict the peak reverse recovery current as a function of the diode parameters [27]. The model suggests that the plot of against the peak reverse recovery current ($I_{RR}$) will yield a straight line. Figure 10 shows this plot using the experimental measurements at 3 different temperatures where a constant slope can be observed, as predicted by the model. The slope of this line yields the parameter $k_Q$ which relates the charge stored in the diode during the conduction of the forward current to the forward current [1]. Hence, if $k_Q$ is experimentally extracted for a specific diode, the $I_{RR}$ used in the model can be substituted by the $I_{RR}$ in (2). For standard diode 1, $k_Q$ is equal to 15 $C/A^{0.5}$.

### C. Snappiness of the Diode's Reverse Recovery

The snappiness (or sometimes called softness when referring to the opposite of snappiness) of the diode is a measure of how quickly the reverse recovery current of the diode returns to zero from the peak negative value. The snappiness of the diode depends on device parameters like lifetime of minority carriers in the drift region as well as circuit parameters like the switching rate and the diode voltage. Some publications have defined this metric as the ratio of time taken for the current to go from $I_{RR}$ to 0 to the time taken for to go from 0 to $I_{RR}$ [27]. In Figure 3, this is $(t_7 - t_4)/(t_4 - t_2)$. Other publications have defined this metric as the ratio of the *dI/dt* of the positive slope (as the current goes from $I_{RR}$ to 0) and the negative slope (as the current goes from 0 to $I_{RR}$) in reverse recovery [31] or $(dI_{RR}/dt)/(dI_{TF}/dt)$. Generally, snappy diodes are known to switch more quickly, have less switching energy however can have reliability, voltage spike and EMI problems. Soft-recovery diodes generally have higher switching energy although are less of a reliability concern. Here, the dependency of the diode softness on temperature has been assessed by the experimental measurements. The softness factor here is calculated as the ratio of $dI_{RR}/dt$ to $dI_{TF}/dt$ meaning that a small number is a snappy whereas a large number is soft. The measurements presented in Figure 11 show that the snappiness of the diode increases with temperature and with the switching rate similar to what has been stated in [32]. Similar results of increased diode snappiness with turn-OFF $dI_{TF}/dt$ can also be observed in [32].

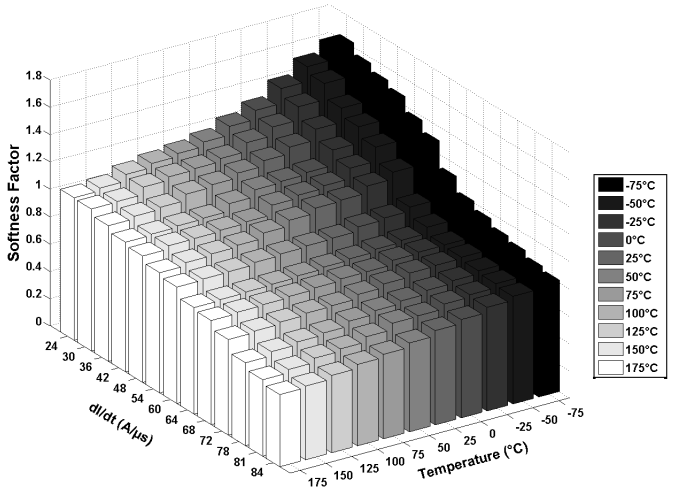


Fig. 11. Softness Factor as a function of the switching rate and temperature

## IV. Model Validation and Application

The model output has been validated by comparison with the experimental measurements through current commutation between the low side IGBT and the high side PiN diode in the inductive clamped switching rig. The validity of the model is tested by applying it to 3 PiN diodes with different characteristics; an ultra-fast diode rated at 1.2 kV and 30 A and two standard recovery PiN diodes rated at 1.2 kV and 40 A and 45 A, respectively; which have been experimentally characterized at different switching rates modulated by gate resistance ranging between 10 Ω to 1000 Ω and temperatures between –75 °C and 175 °C. Figure 12 shows a 3-D plot of the measured diode switching energy as a function of the switching rate (gate resistance switching the low side IGBT) and temperature for standard diode 1 (IXYS DSI45-12A). It can be seen in Figure 12 that the switching energy is lowest at intermediate switching rates. At high switching rates, the switching energy increases due to high peak reverse recovery currents and high peak diode voltage overshoots. Hence, the switching power pulse is high. At slow switching rates, the peaks are reduced however; the width of the switching pulse is large. Hence, the optimal switching rate is intermediate. The switching energy also increases with increasing temperature.

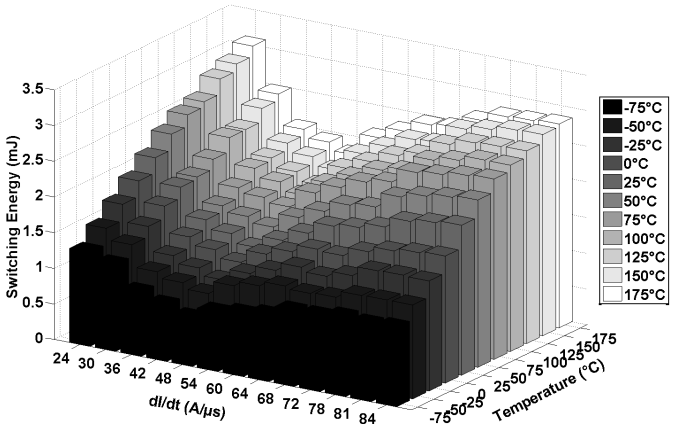


Fig. 12. The turn-OFF switching energy of the diode as a function of the *dI/dt* and the temperature for 100 V and 30 A measurements.

The measurements are also repeated on an ultrafast diode with superior performance. The reverse recovery of the diodes used to validate the model are shown in Figure 13 where the reduced reverse recovery charge of the ultra-fast diode can be observed relative to the standard diodes. Next, the ability of the model to correctly predict the trend seen in Figure 12 is examined. The simplified model was parameterized using the experimental measurements. The inputs to the model included the measured turn-OFF and reverse recovery *dI/dt*, the *dV/dt*, the forward current, the peak reverse current, the temperature dependencies of the peak reverse current, $dI_{TF}/dt$ and diode voltage overshoot as well as other diode parameters like the on-state voltage drop. Figure 14(a) shows the results of the comparison between the experimental measurements and the models developed for calculating the switching energy. As can be seen from Figure 14(a), the proposed model correctly predicts the turn-OFF switching energy of the PiN diode including the minimum switching energy. Figure 14(a) shows the measured switching energy of the 3 devices on a logarithmic basis and as a function of the switching rate whereas Figure 14(b) shows modeled results. This plot is on logarithmic basis to present the behaviour of the model for standard recovery and ultrafast diodes while Figure 15 presents it in a non-logarithmic mode only for the standard recovery diode 1. It can be seen that the calculated switching energy of the model is within 20% margin of error of the experimentally measured switching energies. As the model is considering a non-oscillation mode for the reverse recovery transient, in the ultrafast diodes and especially in colder ambients, the accuracy of the model output might slightly be impacted as the

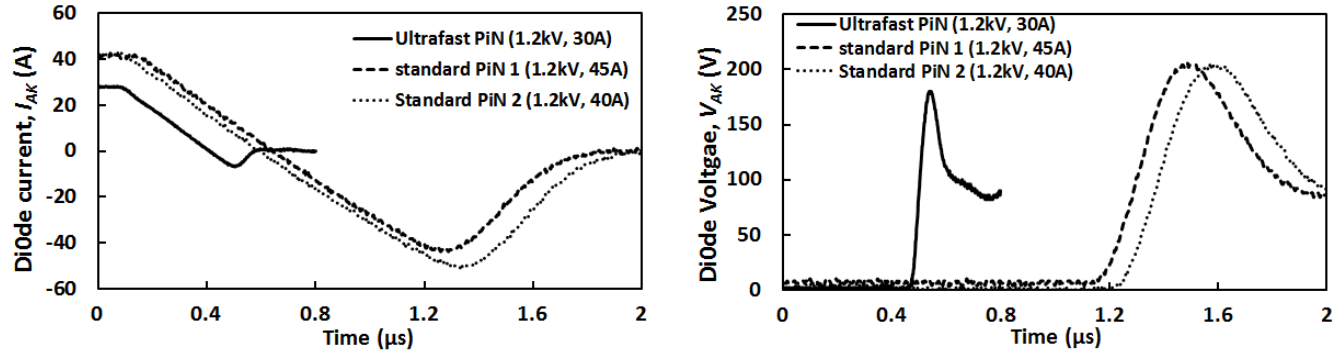


Fig. 13. Reverse recovery and voltage overshoot of 3 PiN Diodes used for validation of the model with $R_G$ = 10 Ω at 25 °C presented on a logarithmic basis.

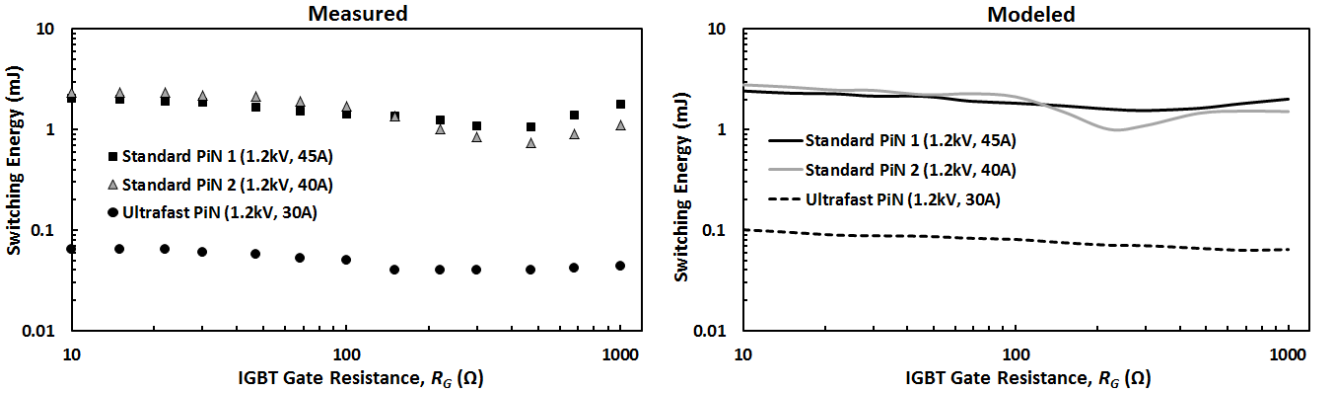


Fig. 14. Measured and Modeled switching energy as a function of the gate resistance performed at room temperature (25 °C) for 3 different PiN Diodes presented on a logarithmic basis.

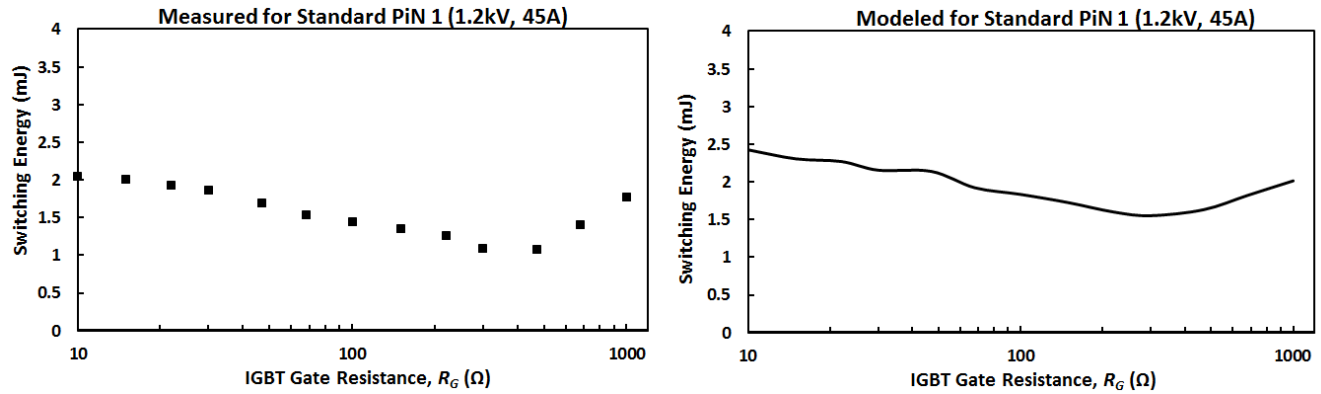


Fig. 15. Measured and Modeled switching energy as a function of the gate resistance performed at room temperature (25 °C) presented on a non-logarithmic basis.

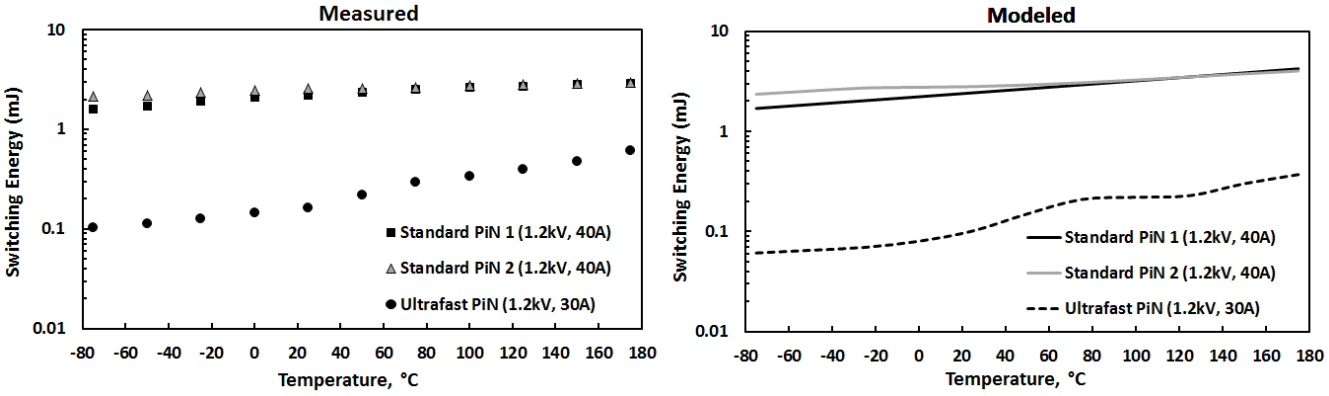


Fig. 16. Measured and Modeled switching energy as a function of the temperature (with $R_G$ = 10 Ω for 3 different PiN Diodes) presented on a logarithmic basis.

these reverse recovery in such conditions might be subject to some oscillations. However, as these oscillations are normally small (when compared to the peak reverse recovery), the portion of the switching energy they represent is significantly smaller compared to the actual reverse recovery waveform. The Silicon Carbide Schottky diodes also present oscillations during turn-OFF and as the model is not designed to predict such conditions, it cannot account for their switching energy. However, it can be used to predict the switching energy of the body diode of power MOSFETs as due to their P-N junction, they also present the reverse recovery phenomenon. Figure 16(a) shows the measured switching energy as a function of temperature for the same devices switched with a gate resistance of 10 Ω whereas Figure 16(b) shows the calculated switching energy derived from the model. Again, it can be seen that the calculated and measured switching energies are within an acceptable margin of error.

## V. Conclusion

An accurate analytical model has been developed that correctly emulates the measurements of PiN diode switching energies as a function of the switching rate and temperature. The model is capable of correctly predicting the switching energy of PiN diodes switched at different rates, different temperatures and can account for non-linear current *dI/dt* that occur at low switching rates. Measurements of current commutation between a low side IGBT and a high side PiN diode at different switching rates and temperatures have shown that the switching energy at high switching rates is dominated by the peak reverse recovery current and diode voltage overshoot. At low switching rates, the switching energy is dominated by the duration of the switching transient. Measurements also show that the slope of the diode's recombination current is as critical as reverse recovery in determining the switching energy because the diode is in recombination at the time when the diode voltage is at its peak. The model developed is validated through experimental measurements on a range of switching rates and temperatures using 3 discrete devices and the outputs are showing a good agreement with the measurements. The model can be used as a diagnostic tool for predicting the switching performance of PiN diodes.

## References

[1] O. Al-Naseem, R. Erickson, and P. Carlin, "Prediction of switching loss variations by averaged switch modeling," in *IEEE Appli. Power Electron. Conf. Expo., APEC 2000. 15th*, vol. 1, 2000, pp. 242–248.

[2] H. Niwa, G. Feng, J. Suda, and T. Kimoto, "Breakdown characteristics of 15-kv-class 4h-sic pin diodes with various junction termination structures," *IEEE Trans. Elect. Devic.*, vol. 59, no. 10, pp. 2748–2752, 2012.

[3] G. Buiatti, F. Cappelluti, and G. Ghione, "Physics-based pin diode spice model for power-circuit simulation," *IEEE Trans. Indust. Applic.*, vol. 43, no. 4, pp. 911–919, 2007.

[4] C. Ma and P. Lauritzen, "A simple power diode model with forward and reverse recovery," *IEEE Trans. Power Electron.*, vol. 8, no. 4, pp. 342–346, 1993.

[5] A. Bryant, L. Lu, E. Santi, P. Palmer, and J. Hudgins, "Physical modeling of fast p-i-n diodes with carrier lifetime zoning, part i: Device model," *IEEE Trans. Power Electron.*, vol. 23, no. 1, pp. 189–197, 2008.

[6] L. Lu, A. Bryant, E. Santi, P. Palmer, and J. Hudgins, "Physical modeling of fast p-i-n diodes with carrier lifetime zoning, part ii: Parameter extraction," *IEEE Trans. Power Electron.*, vol. 23, no. 1, pp. 198–205, 2008.

[7] B. Allard, H. Garrab, T. ben Salah, H. Morel, K. Ammous, and K. Besbes, "On the role of the nn+ junction doping profile of a pin diode on its turn-off transient behavior," *IEEE Trans. Power Electron.*, vol. 23, no. 1, pp. 491–494, 2008.

[8] H. Zhang and J. Pappas, "A moving boundary diffusion model for pin diodes," *IEEE Trans. Magn.*, vol. 37, no. 1, pp. 406–410, 2001.

[9] A. Bryant, X. Kang, E. Santi, P. Palmer, and J. Hudgins, "Two-step parameter extraction procedure with formal optimization for physics-based circuit simulator igbt and p-i-n diode models," *IEEE Trans. Power Electron.*, vol. 21, no. 2, pp. 295–309, 2006.

[10] H. Garrab, B. Allard, H. Morel, K. Ammous, S. Ghedira, A. Amimi, K. Besbes, and J. M. Guichon, "On the extraction of pin diode design parameters for validation of integrated power converter design," *IEEE Trans. Power Electron.*, vol. 20, no. 3, pp. 660–670, 2005.

[11] K. Mayaram, B. Tien, C. Hu, and D. Pederson, "Simulation and modeling for soft recovery of p-i-n rectifiers," in *IEEE Electr. Devic. Meet., IEDM '88. Techni. Digest., Inter.*, 1988, pp. 622–625.

[12] A. Strollo, "Spice modeling of power pin diode using asymptotic waveform evaluation," in *IEEE Power Electron. Special. Conf., PESC '96 Record., 27th*, vol. 1, 1996, pp. 44–49 vol.1.

[13] H. Wang, J. Liu, R. Wang, and Q. Hou, "Modeling diode reverse recovery and corresponding implementation in fast time-domain simulation," in *IEEE Power Electro., ICPE '07. 7th Inter. Conf.*, 2007, pp. 871–875.

[14] A. Maxim and G. Maxim, "A novel power pin diode behavioral spice macromodel including the forward and reverse recoveries and the self-heating process," in *IEEE Appli. Power Electr. Conf. and Expo, APEC 2000. 15th*, vol. 2, 2000, pp. 1088–1094 vol.2.

[15] R. Azar, F. Udrea, M. De Silva, G. Amaratunga, J. Ng, F. Dawson, W. Findlay, and P. Waind, "Advanced spice modeling of large power igbt modules," *IEEE Trans. Indust. Applic.*, vol. 40, no. 3, pp. 710–716, 2004.

[16] Y.-C. Liang and V. Gosbell, "Diode forward and reverse recovery model for power electronic spice simulations," *IEEE Trans. Power Electron.*, vol. 5, no. 3, pp. 346–356, 1990.

[17] S. Pendharkar, M. Trivedi, and K. Shenai, "Dynamics of reverse recovery of high-power p-i-n diodes," *IEEE Trans. Elect. Devic.*, vol. 43, no. 1, pp. 142–149, 1996.

[18] H. Behjati and A. Davoudi, "Reliability analysis framework for structural redundancy in power semiconductors," *IEEE Trans. Ind. Electron.*, vol. 60, no. 10, pp. 4376–4386, 2013.

[19] D. Jones and R. Erickson, "Analysis of switching circuits through incorporation of a generalized diode reverse recovery model into state plane analysis," *IEEE Trans. Circ. Syst.*, vol. 60, no. 2, pp. 479–490, 2013.

[20] A. Bazzi, P. Krein, J. Kimball, and K. Kepley, "Igbt and diode loss estimation under hysteresis switching," *IEEE Trans. Power Electron.*, vol. 27, no. 3, pp. 1044–1048, 2012.

[21] S. Musumeci, A. Raciti, F. Frisina, M. Melito, and M. Saggio, "Performance analysis of merged p-i-n-schottky diodes with doping compensation of the drift region," *IEEE Trans. Ind. Applic.*, vol. 43, no. 3, pp. 636–647, 2007.

[22] J. Biela, M. Schweizer, S. Waffler, and J. Kolar, "Sic versus si;evaluation of potentials for performance improvement of inverter and dc dc converter systems by sic power semiconductors," *IEEE Trans. Ind. Electron.*, vol. 58, no. 7, pp. 2872–2882, 2011.

[23] Y. Xiong, S. Sun, H. Jia, P. Shea, and Z. Shen, "New physical insights on power mosfet switching losses," *IEEE Trans. Power Electron.*, vol. 24, no. 2, pp. 525–531, 2009.

[24] J. Fu, Z. Zhang, Y.-F. Liu, and P. Sen, "Mosfet switching loss model and optimal design of a current source driver considering the current diversion problem," *IEEE Trans. Power Electron.*, vol. 27, no. 2, pp. 998–1012, 2012.

[25] M. Rodriguez, A. Rodriguez, P. Miaja, D. Lamar, and J. Zuniga, "An insight into the switching process of power mosfets: An improved analytical losses model," *IEEE Trans. Power Electron.*, vol. 25, no. 6, pp. 1626–1640, 2010.

[26] P. Haaf and J. Harper, "Understanding diode reverse recovery and its effect on switching losses," *Fairchild Power Seminar*, pp. A23–A33, 2007.

[27] Y. Wang, Q. Zhang, J. Ying, and C. Sun, "Prediction of pin diode reverse recovery," in *IEEE Power Electro. Special. Conf., PESC 04. 35th*, vol. 4, 2004, pp. 2956–2959 Vol.4.

[28] S. Jahdi, O. Alatise, P. Alexakis, L. Ran, and P. Mawby, "The impact of temperature and switching rate on the dynamic characteristics of silicon carbide schottky barrier diodes and mosfets," *IEEE Trans. Ind. Electron.*, vol. PP, no. 99, pp. 1–1, 2014.
[29] S. Jahdi, O. Alatise, R. Bonyadi, P. Alexakis, C. Fisher, L. Ran, and P. Mawby, "An analysis of the switching performance and robustness of power mosfets body diodes: A technology evaluation," *IEEE Trans. Power Electron.*, vol. PP, no. 99, pp. 1–1, 2014.
[30] S. Jahdi, O. Alatise, C. Fisher, L. Ran, and P. Mawby, "An evaluation of silicon carbide unipolar technologies for electric vehicle drive-trains," *IEEE Journ. Emerg. Selec. Topi. in Power Electr.*, vol. 2, no. 3, pp. 1–12, June 2014.
[31] Semikron, "Operation principle of power semiconductors: Reverse recovery behaviour," *Application Manual*, vol. 59, pp. 42–43, 2012.
[32] J. Subhas chandra Bose, I. Imrie, H. Ostmann, and P. Ingram, "Sonic a new generation of fast recovery diodes," *IXYS Semiconductor Application Manual*, pp. 1–6, 2011.

**Saeed Jahdi** (S'10) received the BSc degree in Electrical Power Engineering from University of Science and Technology, Tehran, Iran, in 2005 and the degree of MSc with distinction in Power Systems and Energy Management from City University London, London, U.K., in 2012. Since then, he is pursuing the Ph.D. degree in electrical engineering as a candidate in Power Electronics laboratory of School of Engineering of University of Warwick, U.K. while he has been awarded an energy theme scholarship for the duration of his research. His current research interests include wide band-gap semiconductor devices in high voltage power converters, circuits and applications. Mr. Jahdi is a member of IEEE Power Electronics, IEEE Industrial Electronics and IEEE Electron Devices societies.

**Olayiwola Alatise** received the B.Eng. degree (with first-class honors) in electrical engineering and the Ph.D. degree in microelectronics and semiconductors from Newcastle University, U.K., in 2008. His research focused on mixed-signal performance enhancements in strained Si/SiGe metaloxidesemiconductor field-effect transistors (MOSFETs). In June 2008, he joined the Innovation R&D Department, NXP Semiconductors, as a Development Engineer, where he designed, processed, and qualified discrete power trench MOSFETs for automotive applications and switched-mode power supplies. In November 2010, he became a Science City Research Fellow with the University of Warwick and since August 2012, he is serving as assistant professor of electrical engineering in University of Warwick, U.K. His research interest include investigating advanced power semiconductor materials and devices for improved energy conversion efficiency.

**Li Ran** (M'98-SM'07) received a PhD degree in Power Systems Engineering from Chongqing University, Chongqing, China, in 1989. He was a Research Associate with the Universities of Aberdeen, Nottingham and Heriot-Watt, at Aberdeen, Nottingham and Edinburgh in the UK respectively. He became a Lecturer in Power Electronics with Northumbria University, Newcastle upon Tyne, the UK in 1999 and was seconded to Alstom Power Conversion, Kidsgrove, the UK in 2001. Between 2003 and 2012, he was with Durham University, Durham, the UK. He joined the University of Warwick, Coventry, UK as a Professor in Power Electronics - Systems in 2012. His research interests include the application of Power Electronics for electric power generation, delivery and utilisation.

**Philip Mawby** (S'85-M'86-SM'01) received the B.Sc. and Ph.D. degrees in electrical engineering from the University of Leeds, U.K., in 1983 and 1987, respectively. His Ph.D. thesis was focused on GaAs/AlGaAs heterojunction bipolar transistors for high-power radio frequency applications at the GEC Hirst Research Centre, Wembley, U.K. In 2005, he joined the University of Warwick, U.K. as the Chair of power electronics. He was with the University of Wales for 19 years and held the Royal Academy of Engineering Chair for power electronics, where he established the Power Electronics Design Center. He has coauthored more than 100 journal and conference papers. His current research interests include materials for new power devices, modeling of power devices and circuits, and power integrated circuits. He is a Chartered Engineer, a Fellow of the Institution of Engineering and Technology, a Senior Member of IEEE and a Distinguished Lecturer for the IEEE Electron Devices Society.